Effects of Voltage Sag on the Performance of Induction Motor Based on a New Transient Sequence Component Method

Dongdong Zhang, *Member, IEEE*, Tianhao Liu, *Member, IEEE*

***Abstract*—Voltage sag is one of the most common power quality disturbances in industry, which causes huge inrush currents in stator windings of induction motors, and adversely impacts the motor secure operation. This paper firstly introduces a 2D Time-Stepping multi-slice finite element method (2D T-S multi-slice FEM) which is used for calculating the magnetic field distribution in induction motors under different sag events. Then the paper deduces the transient analytical expression of stator inrush current based on the classical theory of AC motors and presents a separation method for the positive, negative and zero sequence values based on instantaneous currents. With this method, the paper studies the influences of voltage sag amplitude, phase-angle jump and initial phase angle on the stator positive- and negative-sequence peak currents of 5.5 kW and 55 kW induction motors. This paper further proposes a motor protection method under voltage sag condition with the stator negative-sequence peak currents as the protection threshold, so that the protection false trip can be avoided effectively. Finally, the calculation and analysis results are validated by the comparison of calculated and measured stator peak value of the 5.5 kW induction motor.**

***Index Terms*—Induction motors, instantaneous negative sequence current, time-stepping finite element method, voltage sag.**

I. INTRODUCTION

INDUCTION motors are the most widely used loads in industry [1]-[3]. Power quality issues, such as voltage sag, harmonics, unbalance, overvoltage and so on, may adversely affect the operation of induction motors. Among the above power quality issues, voltage sag has significant impacts on the normal operation of motors. In a sag event, the huge inrush currents in stator winding of motors cause torque ripple, noise and temperature rising and so on. In addition, such huge inrush currents can produce a large voltage drop in transmission line and distribution transformers. Therefore, it is of great importance to study the influences of voltage sag on the motor operation and the characteristics of inrush currents in stator windings, for the secure operation of the motor and power grid.

Voltage sag is defined as a short-duration reduction in rms voltage at a point of the power system which can be caused by a short circuit, overload or starting of electric motors [4]-[5]. In a voltage sag event, the rms voltage drops to 10 to 90 percent of the nominal and lasts for half cycle to one minute [6]-[7]. The characteristics of voltage sag include amplitude, duration, phase-angle jump and initial phase angle [8]-[9]. According to statistics, most voltage sags have a duration of four to ten cycles, and phase-angle jump of -60° to 10° [10]-[12]. Previous literature mainly uses experimental and analytical methods to study the influences of voltage sags on operating performances of motors [13]-[16]. For example, an analytical approach is presented to analyze the interaction between induction motors and voltage sags, which can quickly assess the influence of induction motors on sag characteristics and avoids time-consuming transient simulations [13]; the assessment of the influence of induction motors on voltage sag characteristics at low voltage buses is studied by an analytical approach, without having to perform transient simulations [14]; experimental study and some calculations on a standard three-phase squirrel-cage motor of 5.5 kW induction motor behavior were carried out, and found that the motor re-acceleration duration and amplitudes is determined by the interaction between motor load, system hot-load pickup, and voltage sag amplitude, besides, in deep sags, stator currents at the beginning of the sag and voltage recovery time can reach levels higher than the direct start values [15]; and in [16], the author presented three charts for motor starting planning according to the amount of voltage drop caused by motor starting, the compliance to the ITIC curve, and the compliance to the IEC flicker meter limits, and these charts can help utility planers to conduct quick and first-cut assessment of a motor starting situation. However, the influences of different characteristics on magnetic flux density distribution, current distribution and peak current are not systematically analyzed. In addition, in some cases, the protection devices of motors may misoperate because of voltage sag's recovery point.

This paper uses simulation method to study the transient characteristics of the motor during sag event. It is well known that three-phase short-circuit is the most severe fault in power

Manuscript was submitted for review on 26, June, 2018.

This work was supported in part by the National Natural Science Foundation of China under Grant51307050.

D. Zhang is with the School of Electrical Engineering, Guangxi University, Nanning, 530004, China (e-mail: dongdongzhang@yeah.net).

T. Liu is with the Department of Electrical and Electronic Engineering, University of Hong Kong, Hong Kong, 999077, China (Corresponding author,e-mail: thliu@eee.hku.hk).

Digital Object Identifier 10.30941/CESTEMS.2019.00042

grid, therefore, the symmetric voltage sag caused by three-phase short-circuit is also considered the most severe sag event [17]-[18]. And there are three types of simulation methods for voltage sag analysis, i.e. waveform-level simulation, dynamic simulation and fault calculation, and the main advantage of waveform-level simulation is that it can provide complete information on the characteristics of the disturbance [19]. Therefore, this paper uses a waveform-level simulation, e. g. FEM [20]-[23], as the main methods, and focuses on the symmetric voltage sags.

In this paper, the magnetic field distribution and the transient characteristics of stator inrush current of the motor under sag event is analyzed, by using 2D T-S multi-slice FEM. And then a new sequence current separation method is used to study the influence of sag characteristics on the stator positive- and negative-sequence peak currents of 5.5 kW and 55 kW induction motors and a new motor protection threshold is proposed based on above analysis. Finally, the calculation and analysis result are verified by the comparison of calculated and measured stator peak value of a 5.5kW induction motor.

II. Motor Transient Performance Calculation Method Based on 2D T-S Multi-Slice FEM

2D T-S multi-slice FEM is suitable for the analysis of transient performances of motors in the case of stator terminal voltage changes. For a motor with skewed rotor, the axial magnetic field is non-uniform. The transient performance can be calculated by using 2D T-S multi-slice FEM, which considers some factors such as skin effect of rotor bars and the magnetic circuit saturation. The transient boundary value problem of the motor can be expressed as follows [23]-[24].

$$\begin{cases} V:\dfrac{\partial}{\partial x}(\dfrac{1}{\mu}\dfrac{\partial A}{\partial x})+\dfrac{\partial}{\partial y}(\dfrac{1}{\mu}\dfrac{\partial A}{\partial y})=-J_s+\sigma\dfrac{\partial A}{\partial t} \\ T:A=0 \end{cases} \tag{1}$$

where V is solved region, T is stator and rotor outer circle boundary, A is nodal magnetic vector potential, J_s is current density, and μ is permeability.

Motor mechanical motion equation can be expressed as

$$\begin{cases} J_m\dfrac{d\Omega}{dt}=T_e-T_m \\ \Omega=\dfrac{d\theta}{dt} \end{cases} \tag{2}$$

where J_m is rotational inertia, Ω is rotor mechanical angular velocity, $d\Omega/dt$ is angular acceleration, T_e is electromagnetic torque, T_m is load torque, and θ is angle of rotor position.

The equation (1) is discretized and combined with the circuit and motion equations, by which field-circuit-motion coupling equation is obtained as [23]-[24]

where k is the number of the slices for skew modelling, $A_{(k)}$ is the nodal magnetic potential vector, $D_{A(k,\theta)}$, $Ds_{(k,\theta)}$, and $Ds_{(k,\theta)}$ are the matrices that correspond to the derivative terms of nodal vector magnetic potential in the field equation, stator and rotor circuit, respectively; $K_{A\ (k,\ \theta)}$ is the stiffness matrix of field equations, I_s is the vector of stator currents, I_r is the vector of rotor current, and U_s is the matrix of supply voltage.

$$\begin{bmatrix} \boldsymbol{K}_{A(1,\theta)} & 0 & 0 & 0 & \boldsymbol{K}_{s(1,\theta)} & \boldsymbol{K}_{r(1,\theta)} & 0 & 0 \\ 0 & \boldsymbol{K}_{A(2,\theta)} & 0 & 0 & \boldsymbol{K}_{s(2,\theta)} & \boldsymbol{K}_{r(2,\theta)} & 0 & 0 \\ 0 & 0 & \cdots & 0 & \cdots & \cdots & 0 & 0 \\ 0 & 0 & 0 & \boldsymbol{K}_{A(k,\theta)} & \boldsymbol{K}_{s(k,\theta)} & \boldsymbol{K}_{r(k,\theta)} & 0 & 0 \\ 0 & 0 & 0 & 0 & \boldsymbol{R}_s & 0 & 0 & 0 \\ 0 & 0 & 0 & 0 & 0 & \boldsymbol{R}_r & 0 & 0 \\ \boldsymbol{A}_{(1)}^{\mathrm{T}}\boldsymbol{H} & \boldsymbol{A}_{(2)}^{\mathrm{T}}\boldsymbol{H} & \cdots & \boldsymbol{A}_{(k)}^{\mathrm{T}}\boldsymbol{H} & 0 & 0 & 0 & 0 \\ 0 & 0 & 0 & 0 & 0 & 0 & 1 & 0 \end{bmatrix} \begin{bmatrix} \boldsymbol{A}_{(1)} \\ \boldsymbol{A}_{(2)} \\ \cdots \\ \boldsymbol{A}_{(k)} \\ \boldsymbol{I}_s \\ \boldsymbol{I}_r \\ \Omega \\ \theta \end{bmatrix} +$$

$$\begin{bmatrix} \boldsymbol{D}_{A(1,\theta)} & 0 & 0 & 0 & 0 & 0 & 0 & 0 \\ 0 & \boldsymbol{D}_{A(2,\theta)} & 0 & 0 & 0 & 0 & 0 & 0 \\ 0 & 0 & \cdots & 0 & 0 & 0 & 0 & 0 \\ 0 & 0 & 0 & \boldsymbol{D}_{A(k,\theta)} & 0 & 0 & 0 & 0 \\ \boldsymbol{D}_{s(1,\theta)} & \boldsymbol{D}_{s(2,\theta)} & \cdots & \boldsymbol{D}_{s(k,\theta)} & \boldsymbol{L}_s & 0 & 0 & 0 \\ \boldsymbol{D}_{r(1,\theta)} & \boldsymbol{D}_{r(2,\theta)} & \cdots & \boldsymbol{D}_{r(k,\theta)} & 0 & \boldsymbol{L}_r & 0 & 0 \\ 0 & 0 & \cdots & 0 & 0 & 0 & -\boldsymbol{J}_m & 0 \\ 0 & 0 & 0 & 0 & 0 & 0 & 0 & -1 \end{bmatrix} \frac{\partial}{\partial t} \begin{bmatrix} \boldsymbol{A}_{(1)} \\ \boldsymbol{A}_{(2)} \\ \cdots \\ \boldsymbol{A}(\boldsymbol{k}) \\ \boldsymbol{I}_s \\ \boldsymbol{I}_r \\ \Omega \\ \theta \end{bmatrix} = \begin{bmatrix} 0 \\ 0 \\ 0 \\ 0 \\ \boldsymbol{U}_s \\ 0 \\ \boldsymbol{T}_m \\ 0 \end{bmatrix} \tag{3}$$

III. Transient Characteristics of the Motor with Symmetrical Voltage Sag Condition

A. The transient characteristic of magnetic fields

Inrush current and electromagnetic torque fluctuations may occur during the voltage sag process. The waveforms of terminal voltage and stator current of a 5.5 kW induction motor under the conditions of 85% rated load and 30% voltage sag are shown in Fig. 1. It can be seen that the peak value of inrush current I_P can reach 4 times the rated current at the initial moment of voltage sag, while the peak value of inrush current I_{PP} may reach 6 times the rated current at the voltage recovery moment. Such large inrush current can cause severe saturation in the local position of iron core, especially the tooth top of stator and rotor. Fig. 2 (a) shows the magnetic flux under normal operation, and Fig. 2 (b) shows the instantaneous field at the moment of half cycle since the voltage sag initial moment. It can be seen that the flux mainly exists in the leakage magnetic path during sag process, and the most saturated area is the tooth top, while it is very sparse in yoke, especially stator yoke, which is non-saturation region.

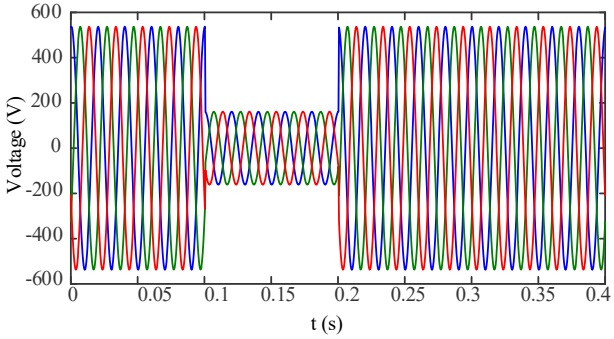

(a) The measured terminal voltage waveform

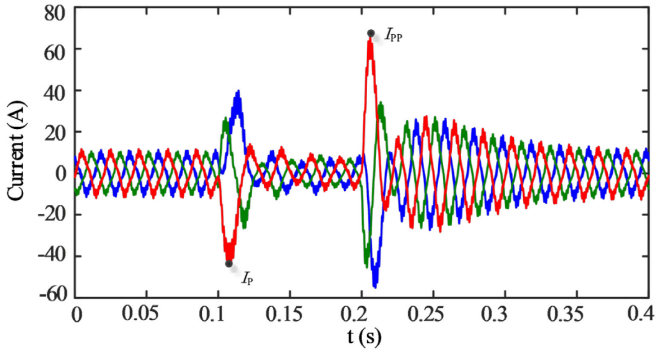

(b) The measured stator current waveform

Fig. 1. Terminal voltage and stator current of the 5.5 kW induction motor with 85% rated load at 30% voltage sag.

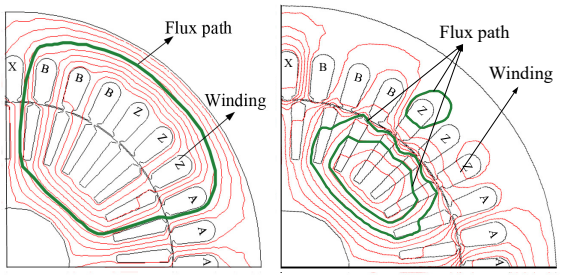

Fig. 2. The magnetic flux of 5.5 kW induction motor with 85% rated load. (Left: The magnetic flux of normal operation; Right: The magnetic flux at half cycle since the 30% voltage sag)

B. The distribution characteristics of magnetic flux density and rotor bar current density

Due to magnetic field distortion and skin effect, the distribution of magnetic flux density in the motor core and current densities in the rotor bar is extremely inhomogeneous during the sag process. The magnetic flux density distribution and rotor bar current density distribution of a 5.5 kW induction motor with 85% rated load under sag and normal operation are shown in Fig. 3. We can conclude that:

1) The magnetic flux density distribution at half cycle since the 30% voltage sag and normal operation of the 5.5 kW induction motor with 85% rated load is shown in Fig. 3 (a) and Fig. 3 (b). Conclusions are listed below:

- At half cycle since the voltage sag, the flux densities on the stator and rotor tooth top regions are obvious higher than that on the yoke regions. For example, as shown in Fig. 3 (a), the flux density in some points of the rotor tooth top areas is higher than 2.7 T, however in most of yoke regions in the flux density is less than 0.5 T.
- Unlike normal operation, the distribution of magnetic flux density in the motor core at half cycle since the voltage sag is extremely inhomogeneous.

2) The rotor bar current density distributions at half cycle since the 30% voltage sag and normal operation of the 5.5 kW induction motor with 85% rated load are shown in Fig. 3 (c) and Fig. 3 (d). Summarizes are shown below:

- Due to skin effect, the current density in the rotor bar top areas far outweigh than the rotor bar middle and bottom areas. For example, as shown in Fig. 3 (c), the current density of the rotor bar top areas is higher than 3.5×10^7 A/m^3, but the current density in most areas of the rotor bar middle and bottom regions is lesser than 0.8×10^7 A/m^3.
- The current density on the rotor bar top regions during the voltage sag is obviously higher than that on at the normal operation. For example, as shown in Fig. 3 (c) and Fig. 3 (d), the current density in some points of the rotor bar top areas reaches 4.1×10^7 A/m^3, at half cycle since the voltage sag, however, at the normal operation, that current density is less than 1×10^7 A/m^3.

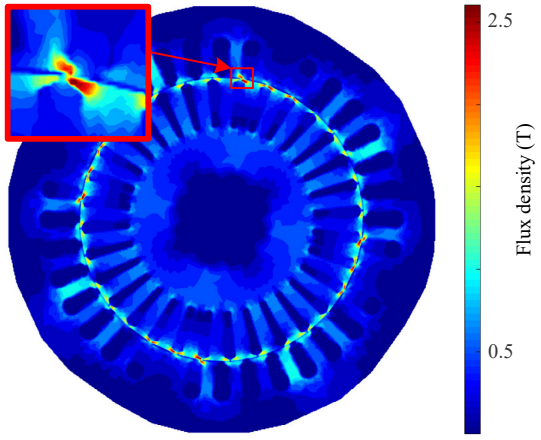

(a) The magnetic flux density distribution (At half cycle since the 30% voltage sag)

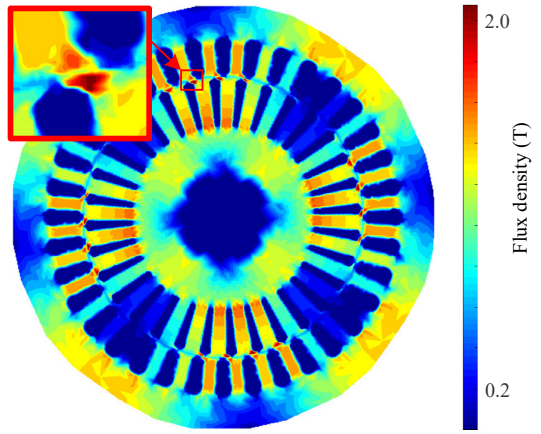

(b) The magnetic flux density distribution (Normal operation)

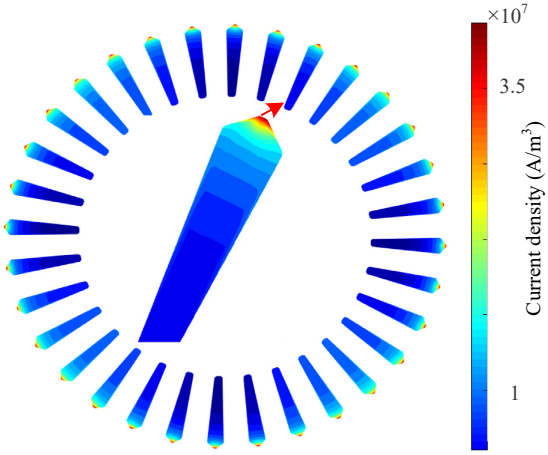

(c) The rotor bar current density distribution (At half cycle since the 30% voltage sag)

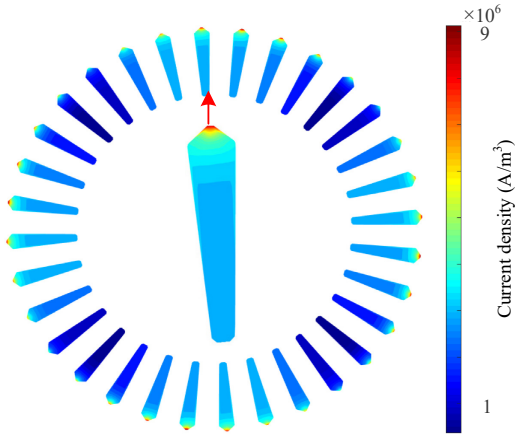

(d) The rotor bar current density distribution (Normal operation)

Fig. 3. The rotor bar current density distribution of 5.5 kW induction motor with 85% rated load.

IV. Solution of Transient Sequence Components During Voltage Sag

A. The solution of transient positive, negative and zero sequence current components

Since it is difficult to use the analytical method to accurately consider the complex nonlinear factors, such as core saturation and harmonic fields, this paper uses 2D T-S multi-slice FEM method mentioned in Section I to calculate the stator current during the voltage sag. And then, the calculated or measured stator current is used to obtain transient positive, negative and zero sequence current component. The solution refers to the transient symmetrical component method in [25]-[26] and the detailed solving process is as follows.

Firstly, the calculated or measured stator current can be divided into positive, negative and zero sequence components, which can be described as follows.

$$I = I^1 + I^2 + I^0 \tag{4}$$

where $I = [i_a, i_b, i_c]^D$; $I^1 = [i_a^1, i_b^1, i_c^1]^D$; $I^2 = [i_a^2, i_b^2, i_c^2]^D$; $I^0 = [i_a^0, i_b^0, i_c^0]^D$; subscripts a, b and c represent the three-phase components; superscripts 1, 2 and 0 are positive, negative and zero sequence; i is the transient current value; I is the matrix comprised of the transient current values; D is the transpose symbol. And the stator positive, negative and zero sequence currents should satisfy (5) and (6).

$$\begin{cases} i_a^2(t) + i_b^2(t) + i_c^2(t) = 0 \\ i_a^2(t + 2T/3) = i_b^2(t + T/3) = i_c^2(t) \end{cases} \tag{5}$$

$$i_a^0(t) = i_b^0(t) = i_c^0(t) = i^0(t) \tag{6}$$

And then, based on Kirchhoff's law, we can obtain

$$i_a^1(t) + i_b^1(t) + i_c^1(t) = 0 \tag{7}$$

From (9) to (12), we can obtain

$$I^0 = \frac{1}{3} L I \quad , \tag{8}$$

where

$$L = \begin{bmatrix} 1 & 1 & 1 \\ 1 & 1 & 1 \\ 1 & 1 & 1 \end{bmatrix} \tag{9}$$

$$I^2(t) = G\left[G_1\left(E - L/3\right) I(t) - \left(E - L/3\right) I(t + T/3)\right] \tag{10}$$

$$I^1(t) = I - I^0(t) - I^2(t) \tag{11}$$

where $E = \begin{bmatrix} 1 & 0 & 0 \\ 0 & 1 & 0 \\ 0 & 0 & 1 \end{bmatrix}$, $G_1 = \begin{bmatrix} 0 & 0 & 1 \\ 1 & 0 & 0 \\ 0 & 1 & 0 \end{bmatrix}$, $G_2 = \begin{bmatrix} 0 & 1 & 0 \\ 0 & 0 & 1 \\ 1 & 0 & 0 \end{bmatrix}$,

$G = (G_1 - G_2)^{-1}$

As to the above solution, some explanations are given as follows.

1) The method of solving negative sequence component by transient current at different moment is different from the traditional method which divides the current phasor into positive, negative and zero sequence space vector components [26].
2) The positive, negative and zero sequence currents in this paper represent the transient time sequence currents, which only borrow the traditional concepts.

B. Solution examples of positive, negative and zero sequence transient currents

With the measured current waveform in Fig. 1 (b), we can obtain positive, negative and zero sequence currents based on the solution mentioned above, as shown in Fig. 4. It can be seen that, at the initial moment of voltage sag, the peak value of positive and negative sequence currents are 45A and 29.6A, respectively. And at the voltage recovery moment, they are 64.6A and 32.1A, respectively. Obviously, the peak values of negative sequence current at the initial moment of voltage sag and voltage recovery moment are closed to each other. Furthermore, the zero-sequence current can be neglected due to its small value.

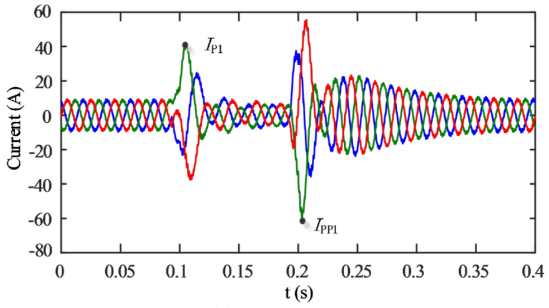

(a) Positive sequence current

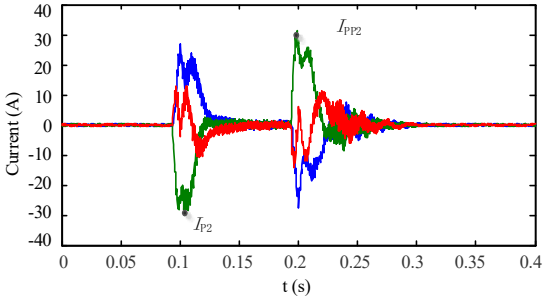

(b) Negative sequence current

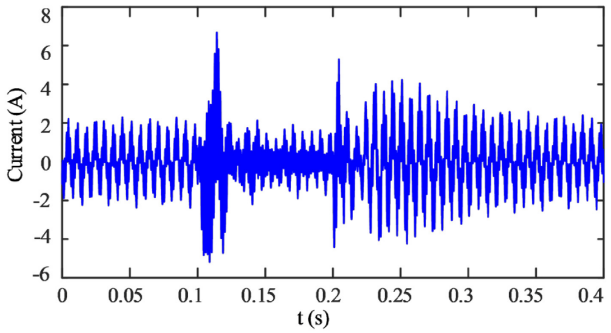

(c) Zero sequence current

Fig. 4. Stator positive, negative and zero current components of the 5.5 kW induction motor with 85% rated load at 30% voltage sag.

V. The Characteristics of Transient Positive and Negative Sequence Current and its Applications in Motor Protection

A. Influence of sag amplitude on the peak values of transient positive and negative sequence current

Since most of voltage sag durations are 4 to 10 cycles, the motor speed can be assumed as constant during this period due to the big inertial. With the 5.5 kW and 55 kW induction motors at no-load or 85% rated load, this paper mainly studies the influence of sag amplitude, sag phase-angle jump and sag initial phase angle on peak value of the stator transient currents under symmetrical sag conditions.

To study the influence of sag amplitude on the peak currents of transient positive and negative sequence currents, it can be assumed to set phase-angle jump and initial angle of phase A voltage of the sag to 0° and the sag duration to 100ms. The only variable is the sag amplitude. The peak values of the positive and negative sequence currents with sag amplitudes from 10% to 90% are shown in Fig.5 and Fig.6. It is shown that

1) Positive sequence and negative sequence peak currents, especially negative sequence, increase almost linearly with sag amplitude increasing.
2) The positive sequence and negative sequence peak currents with and without load have little difference. And the peak values of negative sequence peak currents vary within 10% at load and no-load conditions.

B. Influence of sag angle jump on the peak currents of transient negative sequence

To study the influence of sag phase-angle jump on the peak currents of transient positive and negative sequence, it can be assumed to keep the voltage amplitude constant and set the sag initial phase angle of phase A voltage to 0° and the sag duration to 100ms, only the sag phase-angle jump can be changed. To make conditions close to the real sag situation of the grid, this paper focuses on the sag phase-angle jump of -60° to 10°. The variation of peak values of stator positive and negative sequence currents with the sag phase-angle jump is shown in Fig.7 and Fig.8. It can be seen that

1) The voltage sag phase-angle jump results in a large stator positive and negative sequence inrush current, even larger than the inrush currents caused by sag amplitude. With the 5.5 kW motor, I_{P1}, I_{PP1}, I_{P2} and I_{PP2} are 62.5A, 74.5A, 40.4A and 39.8A, respectively, when sag amplitude is 10%, as shown in Fig.5 (a); and I_{P1}, I_{PP1}, I_{P2} and I_{PP2} are 75.5A, 87.4A, 49.6A and 50.4A, respectively, when voltage sag phase-angle jump is -60°, as shown in Fig.7 (a).
2) The positive and negative sequence peak currents increase linearly with sag phase-angle jump, and the peak values of negative sequence peak currents vary within 10% at load and no-load conditions, as shown in Fig.7 and Fig.8.

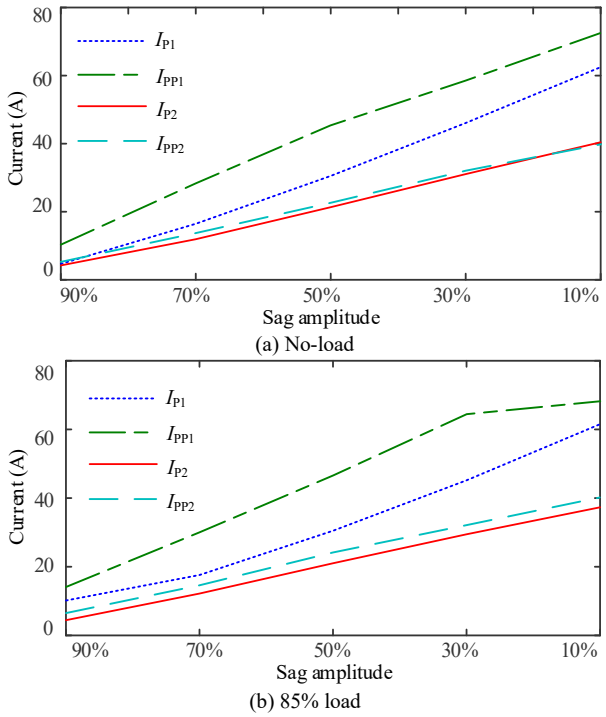

(a) No-load

(b) 85% load

Fig. 5. The variation of the positive and negative sequence peak currents of the 5.5 kW motor with sag amplitude

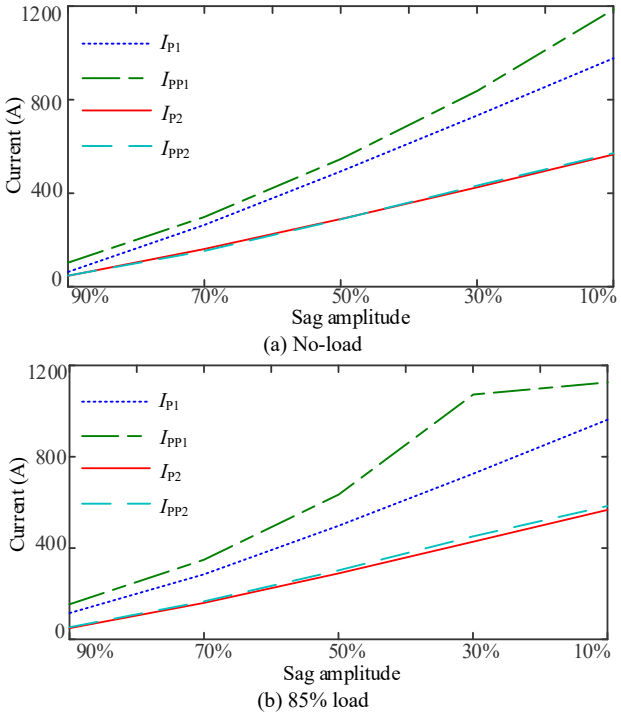

(a) No-load

(b) 85% load

Fig. 6. The variation of the positive and negative sequence peak currents of the 55 kW motor with sag amplitude

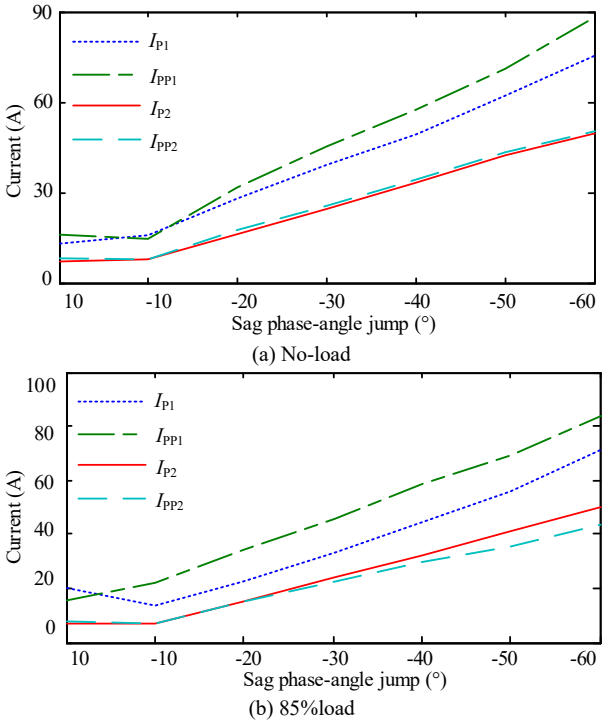

Fig. 7. The variation of the positive and negative sequence peak currents of a 5.5 kW motor with the sag phase-angle jump

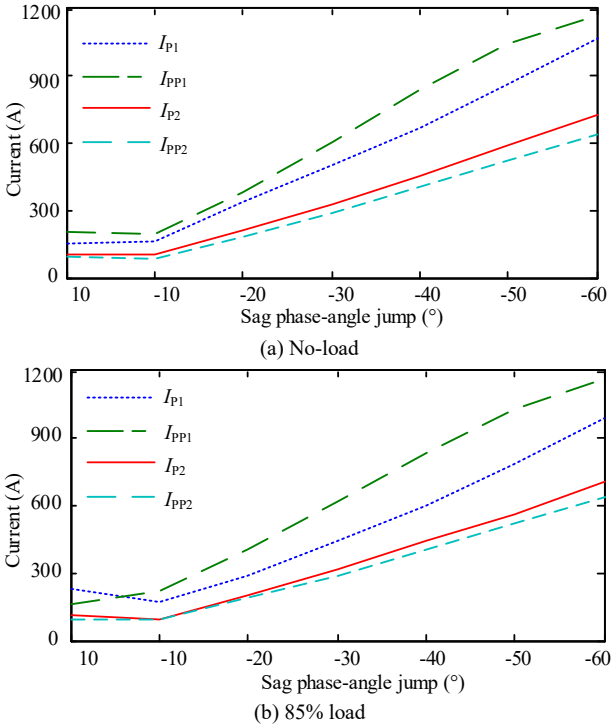

Fig. 8. The variation of the positive and negative sequence peak currents of a 55 kW motor with the sag phase-angle jump

C. *Influence of the sag initial angle on peak currents of transient negative sequence*

To study the influence of sag initial phase angle on the peak currents of transient positive and negative sequence, it can be assumed to set the sag phase-angle jump to 0°, the sag duration to 100ms and the sag amplitude to 30%. The initial phase angle of phase A is the only variable. The variation of stator positive and negative sequence peak currents with sag initial phase angle is shown in Fig.9 and Fig.10.

It can be seen that the sag initial phase angle results in little change in the positive and negative sequence peak currents, for the 5.5kW and 55kW motor, and the fluctuations of the positive and negative sequence peak currents with the sag initial phase angle are within 10%, and the peak values of negative sequence peak currents also vary within 10% at load and no-load conditions.

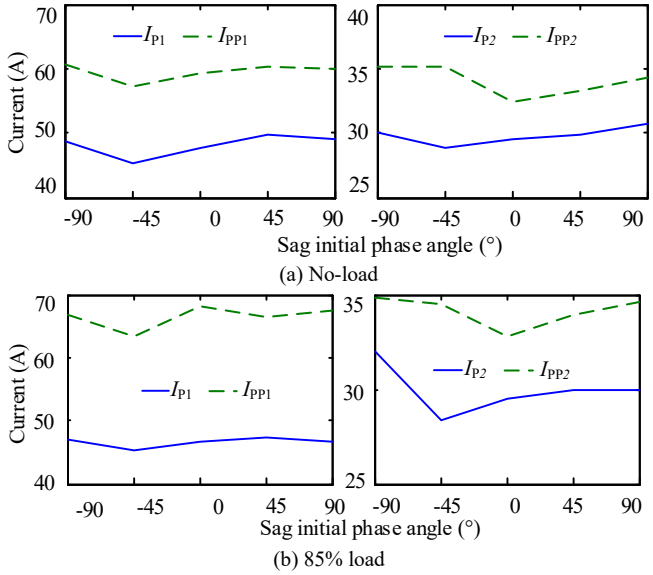

Fig. 9. The variation of positive and negative sequence peak currents of the 5.5 kW motor with the sag initial phase angle

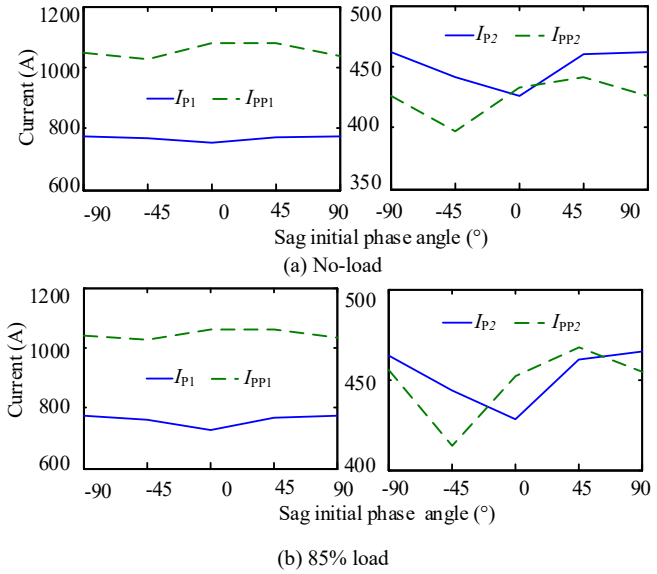

Fig. 10. The positive sequence and negative sequence peak currents of a 55 kW motor vary with the sag initial phase angle

D. *The new motor protection threshold base on transient negative sequence currents*

In summary, transient positive sequence and negative sequence peak currents have follow characteristics.

1) The peak values of transient negative sequence currents vary within 10% at the initial and recovery moments of the voltage sag.

2) The peak values of transient negative sequence currents increase linearly with the increase of the voltage sag amplitude and sag phase-angle jump.
3) The variation of the positive and negative sequence peak currents caused by the sag initial phase angle is within 10%; and the variation caused by the motor load is also within 10%.

Based on the above characteristics, to avoid the protection false trip by the larger peak currents in voltage recovery moment, the new protection threshold I_{set} can be expressed as (12), where the value of I_{set} at the initial moment of voltage sag is larger than the value of I_{set} at the voltage recovery moment.

$$I_{set} = I_{m2} - (0.15 \sim 0.2)\ I_{m1} \tag{12}$$

where I_{m1}, I_{m2} are the peak values of positive and negative sequence currents during voltage sag, I_{set} is threshold value, which can ensure that I_{set} of peak current at initial point is larger than that of peak current at recovery point. And because the peak values of transient negative sequence currents increase linearly with the increase of the voltage sag amplitude and sag phase-angle jump, therefore, the new motor protection method almost can avoid non-linear calculation effort.

VI. Experimental Verification

A. Test rig

To verify the correctness of analysis above, experimental validation is performed on the 5.5kW motor, as shown in Fig. 11. Chroma 18600 programmable power source with 60kVA rated power is used to generate voltage sag waveform. Power analyzer is used to measure the operating performance under steady-state condition. A torque transducer is used to measure the transient torque and speed, and steady-state torque and speed can be read directly from the torque meter. Meanwhile, the transient waveforms, such as stator current, terminal voltage, torque and speed in voltage sag process, can be recorded by the oscilloscope. In a short period of time, such as voltage sag conditions, the maximum capability of negative sequence currents of the 5.5 kW motor and 55 kW motor are 4.3 and 3.2 times of the rated current, respectively. When the negative sequence currents exceed this value, the performance of the motor and its dives system will be degraded, the life span of the motor will be reduced. However, under experimental conditions, the negative sequence currents exceed this value at the expense of the life span of the motor.

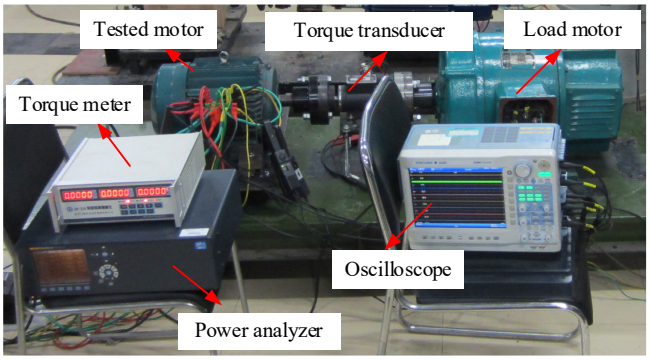

Fig. 11. Test rig.

B. Comparison of the 3D FEM method and 2D T-S multi-slice FEM use in the paper

The comparison of the 3D FEM method (3DM) and 2D T-S multi-slice FEM use in the paper (2DM) is performed by using the 5.5 kW motor under 50% sag magnitude and no-load condition. The 2DM have six layers and each layer has 32406 elements. The 3DM have 96064 elements. Fig. 12 shows the measured current waveform, the current waveform calculated by the 3D M and calculated by the 2DM. We can see that, the calculated current waveform by the 2DM and the 3DM are agree well with the measured waveform. For example, the relative error of the peak current calculated by the 3DM and the 2DM are 2.3% and 2.1%, respectively. From Table I, compared with the 3DM, we can see that the computation time of the 2DM is reduced 93.3%. The 3DM and the 2DM are simulated by a computer with 2 Xeon E5-2690 v3 CPU and 256 GB RAM.

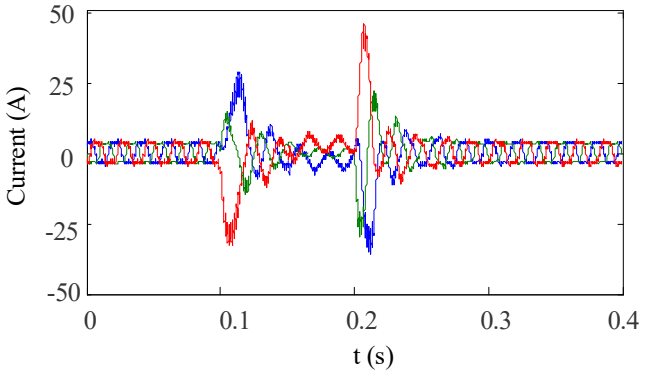

(a) The current waveform calculated by the 3D FEM method

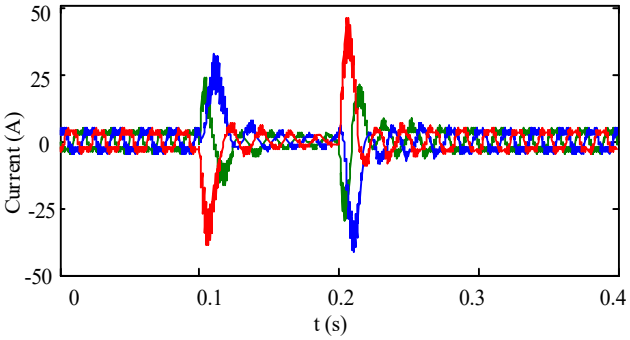

(b) The current waveform calculated by the proposed method

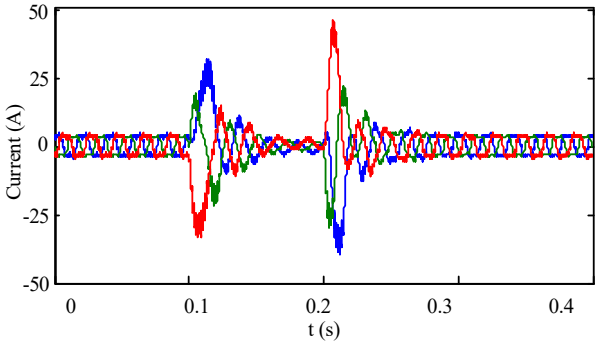

(c) The test current waveform

Fig. 12. Comparison between the measured and calculated stator currents of the 5.5kW induction motor with no-load condition and 50% sag magnitude.

TABLE I
SIMULATION TIME OF THE 3DM AND 2DM

	3DM	2DM
5.5 kW motor	7.8 hours	31.4 minutes

C. Experimental validation

With the 5.5 kW motor under 85% load condition, the measurement and calculation comparisons are given in Fig.13 - Fig.14, the conclusions are as follows.

1) The variation of the measured and calculated peak currents, with voltage sag amplitude and sag phase-angle jump of the, are shown in Fig.13. We can see that the measured and calculated peak values show good agreement.
2) The variation of the measured and calculated peak values of the positive and negative sequence current, with voltage sag amplitude, are showed in Fig.14. Where, I_{MP1}, I_{MPP1}, I_{MP2} and I_{MPP2} represent the measured value of peak current of positive and negative sequence at the initial and recovery moment of the voltage sag, respectively. I_{CP1}, I_{CPP1}, I_{CP2} and I_{CPP2} represent the calculated value, respectively, which also show good agreement.

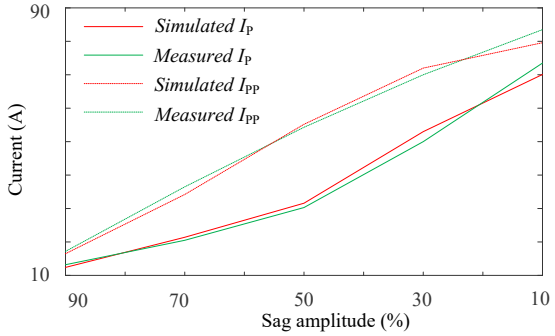

(a) Variation with sag amplitude

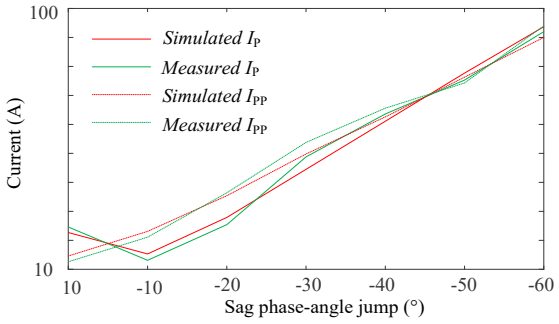

(b) Variation with the sag phase-angle jump

Fig. 13. The measured and calculated peak currents of the 5.5kW induction motor with 85% rated load in sag events.

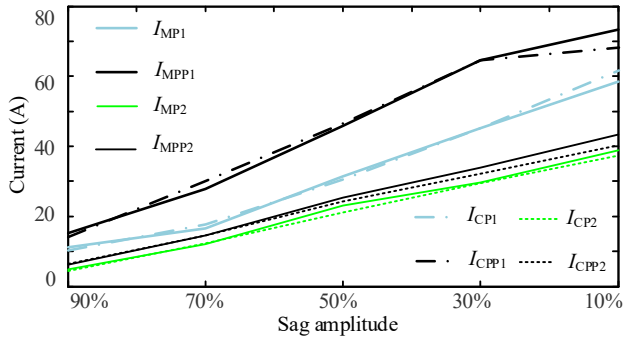

Fig. 14. The measured and calculated transient peak currents of the 5.5kW induction motor with 85% rated load in sag events

D. Experimental results for new protection set point

The traditional protection device usually uses the positive sequence current as the basis of current protection. However, during the process of voltage sag, positive current at recovery point is higher than that at initial point, which may cause the malfunction of protection devices. In this section, we take 55kW motor with 85% load during different sag magnitudes as an example. The current set of protection device is set as 50A. From Fig.15, it can be seen that based on traditional current protection theory, from sag magnitude 25%~45%, the current protection device will active at the recovery point, which will cause the misoperation. However, this problem can be avoid by using the proposed method. As shown in Fig.16, the I_{set} at the initial point always larger than that at the recovery moment, which the misoperation caused by the traditional method can be avoid by using the proposed method.

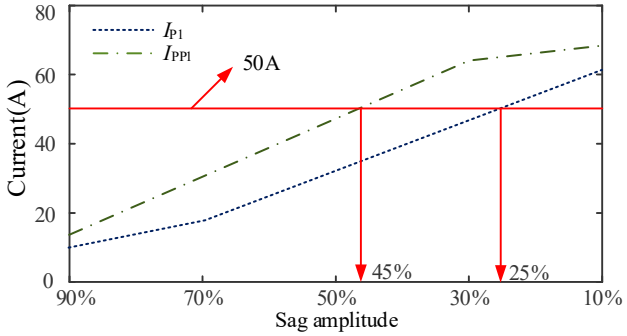

Fig. 15. Traditional current protection method

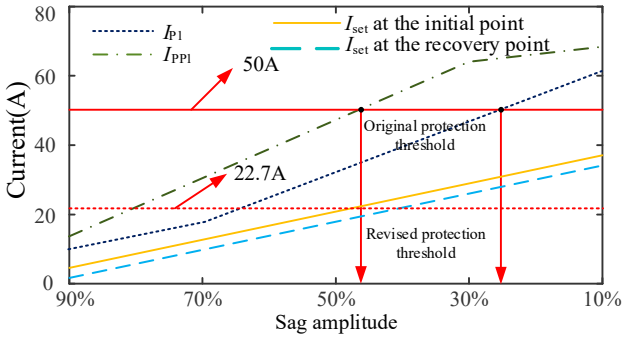

Fig. 16. New current protection method

VII. CONCLUSION

1) The paper studies the characteristics of magnetic field and stator inrush current under different voltage sag condition by using 2D T-S multi-slice FEM, and then presents a separation method for the positive, negative and zero sequence values based on instantaneous currents.
2) The influence of sag amplitude, phase-angle jump, initial phase angle on transient negative sequence peak current of induction motor are analyzed, and a new motor protection threshold is also presented.

The experimental validation is performed on a 5.5kW induction motor, and the correctness of the calculated peak values of the positive and negative sequence current is verified.

REFERENCES

[1] D. Xu, B. Wang, G. Zhang, G. Wang and Y. Yu, “A review of sensorless

control methods for AC motor drives," *CES TEMS*, vol. 2, no. 1, pp. 104-115, Mar. 2018.

[2] S. Wang, Z. Huang, Y. Sun and H. Cao, "Rotor end factors for 2-D FEA of induction motors with smooth or slitted solid rotor," *CES TEMS*, vol. 1, no. 2, pp. 132-139, 2017.

[3] I. Boldea, "Electric generators and motors: An overview," *CES TEMS*, vol. 1, no. 1, pp. 3-14, Mar. 2017.

[4] D. Zhang, T. Liu, C. He and T. Wu, "A new 2-D multi-slice time-stepping finite element method and its application in analyzing the transient characteristics of induction motors under symmetrical sag conditions," *IEEE Access, in press*.

[5] Vanya Ignatova, Pierre Granjon, and Seddik Bacha, "Space vector method for voltage dips and swells analysis," *IEEE Trans. Power Del.*, vol 24, no. 4, pp 2054-2057, Oct. 2009.

[6] *IEEE Recommended Practice for Emergency and Standby Power Systems for Industrial and Commercial Applications*, IEEE Standard 446-1987.

[7] *Voltage Sag Indices – Draft 4*, working document for IEEE 1564, Sep. 2003.

[8] M. H. J. Bollen, *Understanding power quality problems: voltage sags and interruptions*. New York, NY: IEEE, 1995, pp. 153–248.

[9] D. Zhang, R. An and T. Wu, "Effect of voltage unbalance and distortion on the loss characteristics of three-phase cage induction motor," *IET Electrical Appl.*, vol. 12, no. 2, pp. 264-270, Feb. 2018.

[10] Wook-Jin Lee, Seung-Ki Sul, Young-Seok Shim, "A protection scheme against voltage sags for electrolytic capacitorless AC drives with solid salient-pole rotor: performance under starting and voltage sag conditions," *IEEE Trans. Ind. Appl.*, vol. 45, no.1, pp 186-193, Jan. –Feb. 2003.

[11] Xiao Xiangning, Han Mingxiao, etc., *Analysis and control of power quality*. Beijing: China Electric Power Press, 2010: 135-146.

[12] Padmanabh Thakur, Asheesh K. Singh, and Ramesh C. Bansal, "Novel way for classification and type detection of voltage sag," *IET Gener. Transm. Dis*, vol.7, no.4, pp.398 - 404, Apr. 2013.

[13] Jovica V. Milanovic´, Myo T. Aung, and Sarat C. Vegunta, "The influence of induction motors on voltage sag propagation—part I: accounting for the change in sag characteristics," *IEEE Trans. Power Del.*, vol. 23, no. 2, pp 1063-1071, Apr. 2008.

[14] Zhijun Wang, Xiaoyu Wang, and C. Y. Chung, "An analytical method for calculating critical voltage sag clearance time of induction motors," *IEEE Trans. Power Del.*, vol. 27, no. 4, pp 2412-2414, Oct. 2012.

[15] Juan C. Gomez, Medhat M. Morcos, and Claudio A. Reineri, et al, "Behavior of induction motor due to voltage sags and short interruptions," *IEEE Trans. Power Del.*, vol. 17, no. 2, pp 434-439, Apr. 2002.

[16] Xiaoyu Wang, Jing Yong, and Wilsun Xu, etc., "Practical power quality charts for motor starting assessment," *IEEE Trans. Power Del.*, vol. 27, no. 4, pp 2412-2414, Oct. 2012.

[17] Luis Guasch, Felipe Córcoles, and Joaquín Pedra, "Effects of symmetrical and unsymmetrical voltage sags on induction machines," *IEEE Trans. Power Del.*, vol. 26, no. 2, pp 799-807, Apr. 2011.

[18] Alejandro Rol´an, Felipe C´orcoles, and Joaqu´ın Pedra, "Doubly fed induction generator subject to symmetrical voltage sags," *IEEE Trans. Energy Convers.*, vol. 26, no. 4, pp 1219-1229, Nov. 2011.

[19] Xu, Wilsun, "Component modeling issues for power quality assessment," *IEEE Power Engineering Review*, vol.21, no.11, pp 12-17, Nov. 2001.

[20] D. Zhang, H. Dai, H. Zhao and T. Wu, "A fast identification method for rotor flux density harmonics and resulting rotor iron losses of inverter-fed induction motors," *IEEE Trans. Ind. Electron*., vol. 65, no. 7, pp. 5384-5394, Jul. 2018.

[21] Z. Haisen, W. Yilong, Z. Dongdong, Z. Yang, G. X and Y. Luo, "Piecewise variable parameter model for precise analysis of iron losses in induction motors," *IET Electrical Appl.*, vol. 11, no. 3, pp. 361-368, Mar. 2017.

[22] M. M. Nezamabadi, E. Afjei and H. Torkaman, "Design, dynamic electromagnetic analysis, FEM, and fabrication of a new switched-reluctance motor with hybrid motion", *IEEE Trans. on Mag.*, vol. 52, no. 4, pp. 1-8, Apr., 2016.

[23] Y. Huangfu, S. Wang, J. Qiu, H. Zhang, G. Wang and J. Zhu, "Transient performance analysis of induction motor using field-circuit coupled finite-element method," *IEEE Trans. Magn.*, vol. 50, no. 2, pp. 873-876, Feb. 2014.

[24] H. Zhao, D. Zhang, Y. Wang, Y. Zhan and G. Xu, "Piecewise variable parameter loss model of laminated steel and its application in fine analysis of iron loss of inverter-fed induction motors," *IEEE Trans. Ind. Appl.*, vol. 54, no. 1, pp. 832-840, Jan.-Feb. 2018.

[25] Boštjan Polajžer, Gorazd Štumberger, and Drago Dolinar, "Instantaneous positive-sequence current applied for detecting voltage sag sources," *IET Gener. Transm. Dis.*, vol. 9, no. 4, pp 319-327, Mar. 2015.

[26] Tang Yunqiu, Zhang Yihuang, etc., *Transient analysis of AC electric machine*. Beijing: Mechanical Industry Press, 2004: 13-24.

Dongdong Zhang (M'17) was born in Jining, China, in 1990. He received the B.Eng degrees in Electrical Engineering and Automation from the College of Electrical Engineering, Qilu University of Technology, Shandong, China, in 2013, received M. S. Degree in Electric Power System and Automation from North China Electric Power University in 2016, and received Ph.D. degree in Electrical Engineering at the Xi'an Jiaotong University in 2019. Currently, he is an assistant professor with Guangxi University. His research interests include the modeling and optimization of multiple energy system, energy market, and electrical machines and its driving system design.

Tianhao Liu (M'17) was born in Shanxi, China, in 1990. He received the B.Eng degrees and received M. S. degree in electrical engineering and automation from the College of Electrical Engineering, North China Electric Power University in 2013 and 2016, respectively. He worked as an assistant researcher in Southern Power Grid Research Institute in 2017. He is currently working toward the Ph.D. degree in electrical engineering at the Hong Kong University.

His research interests include motor system optimal operation, the modeling and optimization of multiple energy system, and energy market.